Conference paper

Rosario M. P. Colodrero, Inés R. Salcedo, Montse Bazaga-García, Diego F. Milla-Pérez, Jonatan D. Durán-Martín, Enrique R. Losilla, Laureano Moreno-Real, Jordi Rius, Miguel A. G. Aranda, Konstantinos D. Demadis, Pascual Olivera-Pastor and Aurelio Cabeza*

Structural variability in M^{2+} 2-hydroxyphosphonoacetate moderate proton conductors

DOI 10.1515/pac-2016-1003

Abstract: The structural variability of two series of Mg^{2+}- and Zn^{2+}- 2-hydroxyphosphonoacetates have been studied in the range of 25–80 °C and 95% relative humidity in order to correlate the structure with the proton conductivity properties. In addition to selected previously reported 1D, 2D and 3D materials, a new compound, $KZn_6(OOCCH(OH)PO_3)_4(OH)\cdot 5H_2O$ (KZn_6-HPAA-3D), has been prepared and thoroughly characterized. The crystal structure of this solid, solved ab initio from synchrotron X-ray powder diffraction data, consists of a negatively charged 3D framework with K^+ ions, as compensating counterions. It also contains water molecules filling the cavities in contrast to the potassium-free 3D anhydrous $NH_4Zn(OOCCH(OH)PO_3)$ (NH_4Zn-HPAA-3D). In the range of temperature studied, the 1D materials exhibit a 1D → 2D solid-state transition. At 80 °C and 95% RH, the 2D solids show moderate proton conductivities, between 2.1×10^{-5} S·cm^{-1} and 6.7×10^{-5} S·cm^{-1}. The proton conductivity is slightly increased by ammonia adsorption up to 2.6×10^{-4} S·cm^{-1}, although no ammonia intercalation was observed. As synthesized KZn_6-HPAA-3D exhibits a low proton conductivity, 1.6×10^{-6} S·cm^{-1}, attributed to the basic character of the framework and a low mobility of water molecules. However, this solid transforms to the 2D phase, $Zn(OOCCH(OH)PO_3H)\cdot 2H_2O$, upon exposure to dry HCl(g), which enhances the proton conductivity with respect to the as-synthesized 2D material (4.5×10^{-4} S·cm^{-1}). On the other hand, NH_4Zn-HPAA-3D exhibited a higher proton conductivity, 1.4×10^{-4} S·cm^{-1}, than the K^+ analog.

Keywords: coordination polymers; metal phosphonates; POC-16; proton conductivity; solid-state chemistry.

Introduction

There is a growing interest in Metal-Organic Frameworks (MOFs) as proton conductors [1, 2]. Recently, a class of MOFs called metal phosphonates has gained particular attention as potential platforms for proton

Article note: A collection of invited papers based on presentations at the 16th International Conference on Polymers and Organic Chemistry (POC-16), Hersonissos (near Heraklion), Crete, Greece, 13–16 June 2016.

***Corresponding author: Aurelio Cabeza,** Departamento de Química Inorgánica, Universidad de Málaga, Campus Teatinos S/N. 29071-Málaga, Spain, e-mail: aurelio@uma.es
Rosario M. P. Colodrero, Inés R. Salcedo, Montse Bazaga-García, Diego F. Milla-Pérez, Jonatan D. Durán-Martín, Enrique R. Losilla, Laureano Moreno-Real and Pascual Olivera-Pastor: Departamento de Química Inorgánica, Universidad de Málaga, Campus Teatinos S/N. 29071-Málaga, Spain
Jordi Rius: Institut de Ciència de Materials de Barcelona, 08193 Bellaterra, Catalunya, Spain
Miguel A. G. Aranda: CELLS-ALBA synchrotron, Carretera BP 1413, Km. 3.3, E-08290 Cerdanyola, Barcelona, Spain
Konstantinos D. Demadis: Crystal Engineering, Growth and Design Laboratory, Department of Chemistry, University of Crete, Voutes Campus, Crete, GR-71003, Greece

conduction [3] because they exhibit attractive features compared to the well-known carboxylate-based MOFs: (a) Robust frameworks, resistance to hydrolysis and thermal decomposition, (b) Structural diversity, due to the wide selection of phosphonate, carboxyphosphonate, sulfophosphonate, aminophosphonate, etc. linkers, (c) H-bonding networks for proton conduction pathways, (d) Incorporation of a wide variety of metal sites, which can influence coordination number, structure dimensionality, degree of hydration, (e) Presence of acidic sites, e.g. $-PO_3H^-$.

The quest for an "ideal" MOF proton conductor is still on-going, however there are several examples of metal phosphonate materials that are worth-mentioning. We will refer herein to a few recent representative examples, referring the reader to some excellent reviews [3, 4]. Shimizu et al. reported a $[La(H_5L)(H_2O)_4]$ (PCMOF-5, L = 1,2,4,5-tetrakisphosphonomethylbenzene) 3D material that exhibited one of the highest reported proton conductivity values for MOF materials (4×10^{-3} S/cm, at 98 % relative humidity and ~ 60 °C) [5]. The same group reported a proton-conducting MOF, $Mg_2(H_2O)_4(H_2L)\cdot H_2O$ (PCMOF10, H_6L = 2,5-dicarboxy-1,4-benzene-diphosphonic acid) with an extremely high proton conductivity value of 3.55×10^{-2} S/cm at 70 °C and 95 % RH [6]. Zheng et al. reported tunable proton conduction in a mixed metal phosphonate $[Co^{III}Ca^{II}(notpH_2)(H_2O)_2]ClO_4\cdot nH_2O$ [$notpH_6$ = 1,4,7-triazacyclononane-1,4,7-triyl-tris(methylenephosphonic acid)] [7]. Vivani et al. reported high proton conductivity values (1×10^{-3} S/cm at 140 °C and 95 % RH, with a low activation energy of conduction 0.15 eV) for a mixed zirconium phosphate/phosphonate based on glyphosine $(Zr_2(PO_4)H_5(L)_2\cdot H_2O$ [$L = (O_3PCH_2)_2NCH_2COO$] [8]. Krautscheid et al. reported water-mediated proton conduction in a triazolyl phosphonate metal–organic framework $[La_3L_4(H_2O)_6]Cl\times H_2O$ (L^2 = 4-(4H-1,2,4-triazol-4-yl) phenylphosphonate) with highly hydrophilic 1D channels, with a value of 1.7×10^{-4} S/cm^{-1} at 110 °C and in the RH range 20–98 % [9].

These studies, and several others point to a rich variety of structural motifs in proton conducting metal phosphonate MOFs encompassing several metal ions and polyphosphonate, or "mixed" phosphonate ligands. In this paper we report the synthesis, physicochemical characterization, framework interconversions and proton conductivity properties of various divalent metal phosphonates containing the carboxyphosphonate ligand 2-hydroxyphosphonoacetic acid (H_3HPAA). This is part of our continuing work on metal-H_3HPAA MOFs [10–18].

Experimental section

General information

A racemic mixture of *R,S*-2-hydroxyphosphonoacetic acid (50 % w/w stock solution in water), H_3HPAA, was from Biolabs, UK. In-house, deionized (DI) water was used for all syntheses. Stock solutions of HCl, HNO_3 and NaOH were used for pH adjustments. A parallel synthesis procedure was applied to obtain solids by hydrothermal reactions. The autoclave block is made of aluminum and contains six reaction chambers in a 3×2 array. Teflon reactors have an inner diameter of 19 mm and a depth of 18 mm, with a total volume of about 5 mL. A thin sheet of Teflon covers the reaction vessels, which are then sealed inside a specially designed aluminum autoclave. Elemental analyses (C, H, N) were measured on a Perkin–Elmer 240 analyzer. Thermogravimetric analysis (TGA) data were recorded on an SDT-Q600 analyzer from TA instruments. The temperature varied from RT to 1000 °C at a heating rate of 10 °C·min^{-1}. Measurements were carried out on samples in open platinum crucibles under air flow.

Materials syntheses

1D compounds $M^{2+}(OOCCH(OH)PO_3H)\cdot2H_2O$ (M^{2+} = Mg, Zn); M-H_1HPAA-1D were prepared according to literature [14]. $MgCl_2\cdot6H_2O$ (4.39 mmol) or $ZnNO_3\cdot6H_2O$ was added to a solution formed by 1.0 mL of the ligand

stock solution (4.39 mmol) and DI water (25 mL) under vigorous stirring. Solution pH was adjusted to 2.7 with 5.0 M or 1.0 M NaOH stock solutions. The clear, slightly yellow solutions were stored at RT. Microcrystalline materials precipitated after 3 days. The precipitates were isolated by filtration (without washing) and air-dried. Elemental analysis for Mg-H_1HPAA-1D: calculated (wt%): C 11.21, H 3.30; found (wt%): C 10.55, H 3.54, Yield ~ 70 % based on the metal. Elemental analysis for Zn-H_1HPAA-1D: calculated (wt%): C 9.40, H 2.76; found (wt%): C 9.17, H 2.82, Yield ~ 70 % based on the metal.

$Mg(OOCCH(OH)PO_3H)\cdot 2H_2O$, Mg-$H_1$HPAA-2D, was prepared according to literature [14]. $MgCl_2\cdot 6H_2O$ (4.39 mmol) or $ZnNO_3\cdot 6H_2O$ was added to a solution formed by 1.0 mL of the ligand stock solution (4.39 mmol) and DI water (25 mL) under vigorous stirring. Solution pH was adjusted to 2.7 with 5.0 M or 1.0 M NaOH stock solutions. The clear, slightly yellow solutions were stored at RT. After 1 day the precipitates were isolated by filtration (without washing) and air-dried. Elemental analysis for Mg-H_1HPAA-2D: calculated (wt%): C 11.21, H 3.30; found (wt%): C 11.14, H 3.43, Yield ~ 84 % based on the metal.

$Zn(OOCCH(OH)PO_3H)\cdot 2H_2O$, Zn-$H_1$HPAA-2D. A modified, previously reported synthesis was followed [19]. $Zn(OOCCH(OH)PO_3H)(H_2O)_2$ was prepared by dissolving $Zn(OOCCH_3)_2(H_2O)_2$ (11.17 mmol) in a solution formed by 2.5 mL of the ligand stock solution (11.17 mmol) and DI water (25 mL) under vigorous stirring. Solution pH was adjusted to 2.0 with 5 M KOH stock solution. The solution was transferred into a flask and heated under reflux to 100 °C for 72 h. The precipitate was isolated by filtration and air-dried. Elemental analysis for Zn-H_1HPAA-2D: calculated (wt%): C 9.40, H 2.76; found (wt%): C 9.00, H 2.86, Yield ~ 71 % based on the metal.

$KZn_6(OOCCH(OH)PO_3)_4(OH)\cdot 5H_2O$, KZn_6-HPAA-3D. A KOH solution was used for all pH adjustments. A quantity of $Zn(H_2CCOOH)_2\cdot 2H_2O$ (0.4902 g, 2.23 mmol) was added to a solution containing 0.5 mL of the ligand stock solution (2.23 mmol) and 1.5 mL of DI water under stirring. The pH of the resulting solution was 0.74 and it was adjusted to 1, 2.5 or 4.5 with a 4 M stock solution of KOH. A total filling volume of ~ 3 mL per reactor was used. The reaction was conducted at 180 °C for 3 days. The resulting solid was filtered off, washed twice with DI water and acetone, and dried at 50 °C. Elemental analysis for KZn_6-HPAA-3D: calculated (wt%) for $Zn_6KP_4O_{31.5}C_8H_{25.5}$: C 8.35, H 1.66; found (wt%): C 8.664, H 1.375, Yield ~ 85 % based on the metal.

$NH_4Zn(OOCCH(OH)PO_3)$, NH_4Zn-HPAA-3D. A modified literature synthesis was followed [20]. NH_4Zn-HPAA-3D was prepared by dissolving $ZnSO_4\cdot 7H_2O$ (10 mmol) in a solution formed by 2.25 mL of the ligand stock solution (10 mmol) and DI water (20 mL) and NH_4Cl (125 mmol) in DI water (20 mL) under vigorous stirring. Solution pH was adjusted to 2.8 with solid NaOH. The solution was transferred into a flask and heated under reflux to 100 °C for 48 h. The precipitate was isolated by filtration and air-dried. Elemental analysis for NH_4Zn-HPAA-3D: calculated (wt%): C 10.16, H 2.56; N 5.92, found (wt%): C 10.48, H 2.77; N 5.70, Yield ~ 65 % based on the metal.

Post-synthesis modifications with NH_3 and HCl

Adsorption of NH_3 vapors: Based on the derivatization procedure followed in literature [21]. In separate experiments, an amount of 600 mg of Mg-H_1HPAA-1D, or Zn-H_1HPAA-2D or KZn_6-HPAA-3D was placed in contact with vapors from an aqueous solution of 14 wt% of NH_3 for various contact times (17 h for Mg-H_1HPAA-1D; 3.5 h for Zn-H_1HPAA-2D and 1 h for KZn_6-HPAA-3D) in a closed container and then dried for 1 h.
Adsorption of HCl: KZn_6-HPAA-3D (0.3801 g, 0.33 mmol) was exposed to HCl vapors generated from the reaction of an excess of 95 % H_2SO_4 with NaCl for 30 min. After the adsorption reaction the solid was washed with 96 % ethanol, filtered and air-dried. Elemental analysis for: $Mg(HO_3PCHOHCO_2)(H_2O)_{2.6}(NH_3)_{0,2}$, Mg-$H_1$HPAA-1D_$NH_3$, calculated (wt%): C 11.22, H 3.30; N 1.29, found (wt%): C 11.14, H 3.43; N 1.29; $Zn(HO_3PCHOHCO_2)(H_2O)_2(NH_3)$, Zn-$H_1$HPAA-2D_$NH_3$, calculated (wt%): C 8.82, H 5.14; N 3.70, found (wt%): C 8.61, H 5.48; N 3.35.

Structural characterization

Laboratory X-ray powder diffraction (XRPD) patterns were collected on a PANanalytical X'Pert Pro diffractometer equipped with an X'Celerator detector. XRPD patterns corresponding to the single phases were auto-indexed using the DICVOL06 program [22] and the space groups were derived from the observed systematic extinctions. The crystal structure of KZn_6-HPAA-3D was successfully solved following an ab initio methodology. For this purpose, a high resolution synchrotron powder data set was collected on ID31 powder diffractometer of ESRF, European Synchrotron Radiation Facility, (Grenoble, France) using a wavelength $\lambda = 0.2998$ Å selected with a double-crystal Si (111) monochromator and calibrated with Si NIST (a = 5.43094 Å). The Debye-Scherrer configuration was used with the sample loaded in a rotating borosilicate glass capillary of diameter of 1.0 mm. The overall measuring time was ~100 min to have very good statistics over the angular range 1.7–16° (in 2θ). The data from the multi-analyzer Si(111) stage were normalized and summed into 0.003° step size with local software. The integrated intensities extracted with the program Ajust [23] were introduced in the direct methods program XLENS [24]. The starting framework model, containing the totally of atoms in the asymmetric part of the unit cell except those corresponding to the solvent, was derived from the interpretation of the electron density map computed with the set of refined phases with the highest combined figure of merit. The crystal structure was refined by the Rietveld method [25] using the GSAS package [26] and the EXPGUI graphic interface [27]. The following soft constraints were imposed in order to preserve chemically reasonable geometries for the phosphonate, alkyl chain and amine groups. The soft constraints were as follows: PO_3C_1 tetrahedron, P–O [1.53(1) Å], P–C_1 [1.80(1) Å], O···O [2.55(2) Å], O···C_1 [2.73(2) Å]; C_1OH–C_2OO group, C_1–C_2 [1.50(1) Å], C_2–O_{carb} [1.23(1) Å], C_1–OH [1.40(1) Å], P···OH [2.68(2) Å], C_2–OH [2.40(2) Å], O_{carb}···O_{carb} [2.21(2) Å], C_1···Ocarb [2.36(2) Å]. No attempts to locate the H atoms were carried out due to the limited quality of the XRPD data. Two isotropic atomic displacement parameters were fixed for all atoms. Selected structural data are reported in Table 1 and the final Rietveld plot is given in the Supporting Information (SI) as Figure S1.

Thermodiffractometric studies at different relative humidity values were collected on a D8 ADVANCE (Bruker AXS) diffractometer equipped with a Johansson Ge(111) primary monochromator, which gives a strictly monochromatic Mo radiation ($\lambda = 0.7093$ Å), and an Anton Paar MHC-trans chamber. The X-ray tube was operating at 50 kV and 50 mA. The energy-dispersive linear detector LYNXEYE XE 500 μm,

Table 1: Crystallographic data and Rietveld disagreement factors for $KZn_6(OOCCH(OH)PO_3)_4(OH)\cdot 5H_2O$.

Chemical formula	$Zn_6KC_8H_{22}O_{30}P_4$
Formula mass	1168.44
Crystal system	triclinic
Space group	$P\bar{1}$
λ/Å	0.2998
a/Å	14.65217(27)
b/Å	10.15207(18)
c/Å	5.60315(6)
α/°	104.5496(10)
β/°	92.6991(9)
γ/°	103.7705(14)
Unit cell volume/Å^3	778.47(3)
Z	2
Range data (°)	0.003–33.00
Independent reflections	2922
Data/restrains/parameters	6544/47/153
R_{WP}	0.1118
R_P	0.0801
R_F	0.0562
CCDC number	1496547

optimized for high energy radiation, was used with the maximum opening angle. Data were collected at the temperature range 25 and 80 °C and 95 % RH using a heating rate of 1 °C/min. Samples were measured between 2 and 21° (2θ) with a step size of 0.017° and counting time of 154 s/step. Samples were held at each temperature for 10 min before recording any pattern, giving sufficient time for any transformation to take place.

Conductivity characterization

Impedance measurements were carried out on cylindrical pellets (diameter ~5 mm and thickness ~1 mm) obtained by pressing 40 mg of sample at 250 MPa, for 1 min. The pellets were pressed between porous C electrodes (Sigracet, GDL 10 BB, no Pt). The sample cells were placed inside a temperature- and humidity-controlled chamber (Espec SH-222) and connected to a HP4284A impedance analyzer. AC impedance data were collected over the frequency range from 20 Hz to 1 MHz with an applied voltage of 1 V. To equilibrate water content, pellets were first preheated (0.2 °C/min) from 25 to 80 °C and RH 95 %. Impedance spectra were recorded on cooling using a stabilization time of 3 h for each temperature (80, 70, 60, 50, 40, 30, 25 °C). Water condensation on sample was avoided by reducing first the relative humidity before decreasing temperature. All measurements were electronically controlled by the winDETA package of programs [28].

Results and discussion

M^{2+}-H_1HPAA compounds, where M^{2+} = Mg and Zn, can be prepared with different dimensionalities (mono- or bi-dimensional), albeit with the same stoichiometry, $M^{2+}(OOCCH(OH)PO_3H)\cdot 2H_2O$. The purity of all synthesized solids used in this work was checked by X-ray powder diffraction (Figures S2–S6) and elemental analyses. Complete chemical and crystallographic characterization have been carried out for KZn_6-HPAA-3D, reported here by first time. In addition, syntheses of monophasic compounds Mg-H_1HPAA-2D, Zn-H_1HPAA-2D and NH_4Zn-HPAA-3D have been optimized by using shorter treatment times and lower temperatures with respect to those described elsewhere [14, 19, 20].

From a structural point of view, the ligand ($HPAA^{n-}$, n = 1–3) can adopt diverse coordination modes with a wide variety of metal ions [29]. The specific coordination to a metal ion principally depends on the reaction pH and the ionic radius of the metal ion, and may be also influenced by the presence of other ions and/or auxiliary ligands in solution [30, 31]. A fundamental building unit present in many metal-HPAA crystal structures consists of a ligand molecule coordinating simultaneously two metal ions through five- and six-membered chelating rings [10, 11, 14, 32]. These rings are formed by bidentate linkages from (carboxylate, –OH) and (phosphonate, carboxylate) group pairs, respectively. Depending principally (but not exclusively) on the ionic radius of the metal ion, two different configurations may appear (Scheme 1). One, in which the coordination sphere of each metal ion is composed of both chelating rings, and another one, where a central metal atom, from a trimeric unit, forms two six-membered chelating rings around it. The latter is more frequently found in structures constructed with bulky metal ions, such as Ca^{2+} [15, 16, 33].

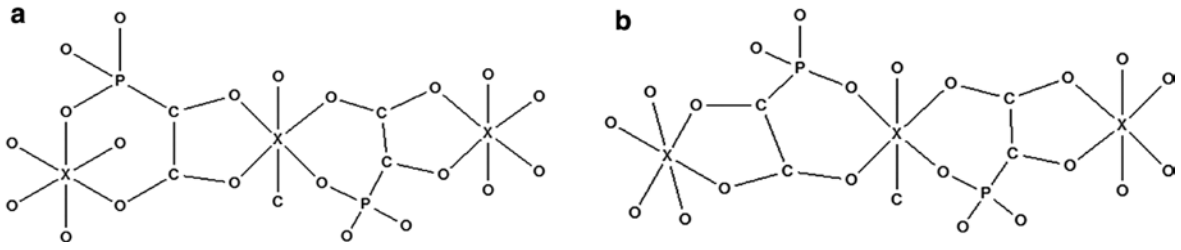

Scheme 1: Usual coordination modes of ligand 2-hydroxyphosphonacetate with metal ions (X).

On this basis, the crystal structure of mono-dimensional M^{2+}-H_1HPAA-1D (M = Mg, Zn) can be described as being composed of alternating five- and six-membered chelating rings around the metal ions (Scheme 1a). The octahedral coordination of these ions is completed by two water molecules, while the carboxylate group bridges two metal centers in a η^2-μ_2-fashion, which results in the formation of infinite 1D chains. On the other hand, 2D structures, are built up with the metal ion exhibiting a coordination similar to that of 1D solids, but increasing the phosphonate-to-metal connectivity, in such a way that each phosphonate group now bridges two M^{2+} ions through two oxygens, while the third oxygen remains uncoordinated [14].

A 1D → 3D structural transformation occurs for M^{2+}-H_1HPAA-1D (M^{2+} = Mg, Zn) by heating the solids under dry conditions. This thermal treatment triggers the loss of the two metal-bound water molecules and causes further dimensionality increase through enhanced phosphonate-to-metal connectivity. As a consequence, the three oxygens of the phosphonate group are now coordinated to M(II) centers and one of them links two M^{2+} ions, generating edge-sharing M_2O_{10} dimers [14].

On the contrary, a 1D → 2D transformation takes place upon heating up to 80 °C and RH > 50 %. Complete conversion was observed after 12 h at 90 % RH (Fig. 1). For this process to happen, water molecules have to remain coordinated to metal ions upon heating. This transformation occurs through rupture of the 6-membered chelate rings by breaking the carboxylate oxygen to metal bond (C–O–M → C–O^- + M) and concomitant linking of adjacent chains through the creation of new phosphonate to metal ion bonds. This results in higher connectivity of the phosphonate groups at the expense of the carboxylate group, whereas the 5-membered chelate rings are preserved (Fig. 2).

Crystal structure $KZn_6(O_3PCHOHCOO)_4(OH)\cdot 5H_2O$ (KZn_6-HPAA-3D). Apart from 1D and 2D architectures, where the ligand $HPAA^{n-}$ is usually partially protonated, 3D frameworks can be generated by hydrothermal syntheses at adequate metal/ligand ratios and higher reaction pHs. These conditions favor higher metal/ligand connectivity and, hence, higher degree of deprotonation of the ligand $HPAA^{n-}$. Following these synthesis criteria, the title compound was isolated by hydrothermal reaction and KOH addition for pH adjustment. The new monophasic compound, KZn_6-HPAA-3D, was isolated at pH 2.5. In solid KZn_6-HPAA-3D, K^+ is thus incorporated into the structure to compensate the negatively charged framework that also contains an OH^- group per formula. Although no absolute configuration could be determined from powder diffraction

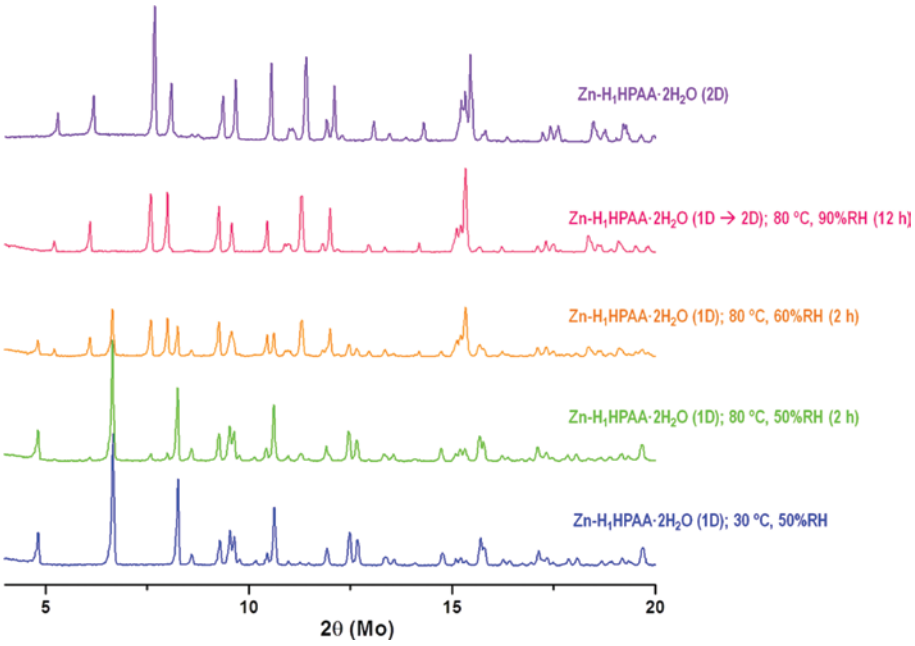

Fig. 1: Diffractometric study for Zn-H_1HPAA-1D showing the transformation 1D → 2D as a function of temperature and relative humidity.

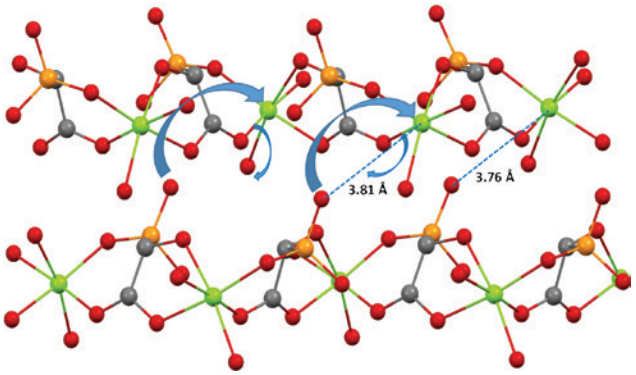

Fig. 2: Schematic representation for the 1D → 2D conversion in M^{2+}-H_1HPAA-1D solids (M^{2+} = Mg, Zn) at high relative humidity.

data, both enantiomers are generally incorporated into the resulting non-chiral networks, except for the case of Cs-HPAA, Cs(HOOCCH(OH)PO_3H), where the *S* enantiomer was exclusively present [18]. This compound crystallizes in the triclinic system $P\bar{1}$ and contains 27 non-hydrogen atoms in the asymmetric unit. There are three crystallographically independent zinc atoms, one-half potassium atom, two fully deprotonated ($HPAA^{3-}$) ligands, one-half hydroxide ion and three water molecules, all of them located in general positions (Fig. 3), but one of them with half occupancy (Ow4).

The framework is built up from organic-inorganic layers (Fig. 4), composed of edge-sharing octahedra dimers, $Zn(1)_2O_{10}$, and $Zn(2)O_4$ tetrahedra linked through $HP(1)AA^{3-}$ and $HP(2)AA^{3-}$ ligands. The former bridges Zn(1) and Zn(2) polyhedra forming 6- (O1 and O5) and 5-membered (O4 and O6) chelate rings, respectively, as previously described. Furthermore, ligand $HP(1)AA^{3-}$ links a second Zn(1) of the dimer through the phosphonate oxygen atom O2 and another Zn(2) atom through the third phosphonate oxygen (O3). Ligand $HP(2)AA^{3-}$ connects Zn(1) forming 5-membered chelate rings (oxygens O10 and O12) and Zn(2) through one phosphonate oxygen (O7), Fig. 4.

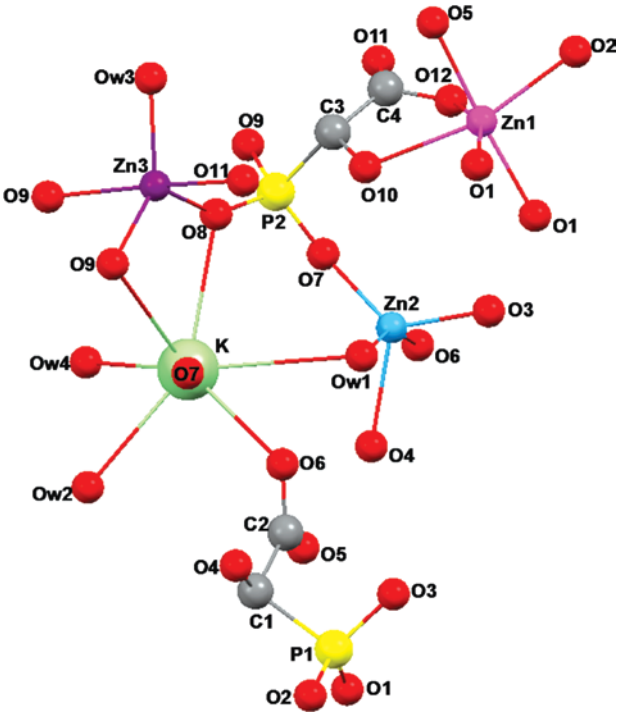

Fig. 3: Content of the extended asymmetric unit of $KZn_6(O_3PCHOHCOO)_4(OH)\cdot 5H_2O$ with atoms labeling.

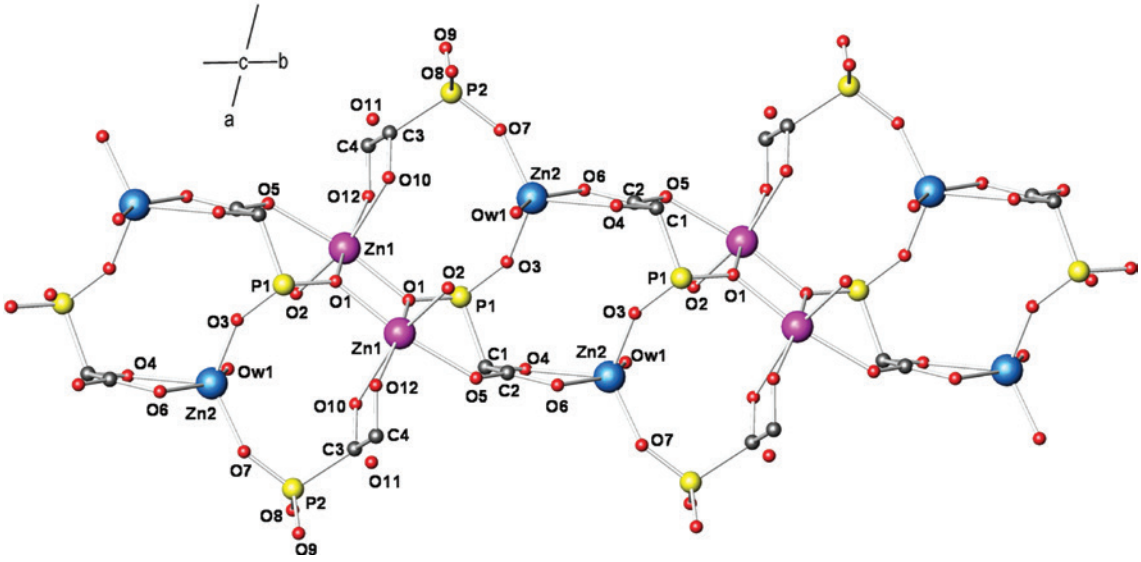

Fig. 4: Detail of the metal-ligand connectivity in KZn_6-HPAA-3D.

The layers are held together by Zn(3) dimers, with distorted trigonal bipyramid coordination and connected through two $HP(2)AA^{3-}$ anions of one layer and another $HP(2)AA^{3-}$ anion from the adjacent layer (Fig. 5). This connectivity creates dimer chains along the *c*-axis (Fig. 6). Dimeric polyhedra are composed of three phosphonate oxygens, from three different phosphonate groups, one carboxylate oxygen and one water molecule. These dimers are connected along the *c*-axis by the phosphonate oxygens O8 and O9. The resulting negatively charged 3D framework is electrostatically neutralized by octa-coordinated K^+ ions. The coordination environment of K^+ is formed by four phosphonate oxygens, from two different $HP(2)AA^{3-}$ ligands and

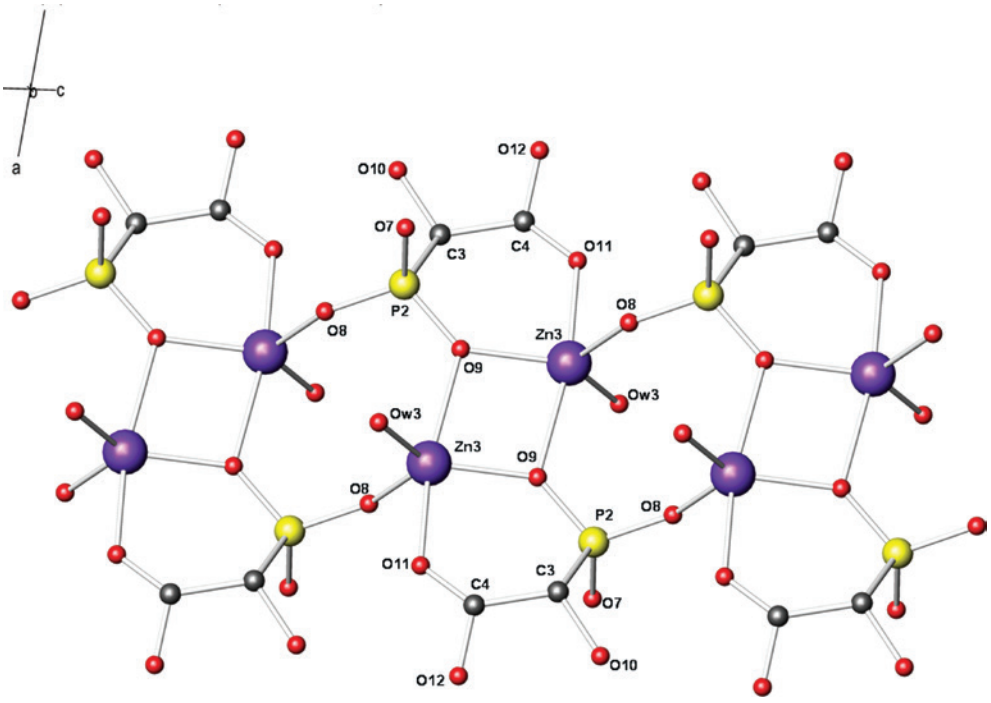

Fig. 5: View of the Zn(3) dimer chains linking the organic inorganic layers through the phosphonate group $HP(2)AA^{3-}$ in KZn_6-HPAA-3D.

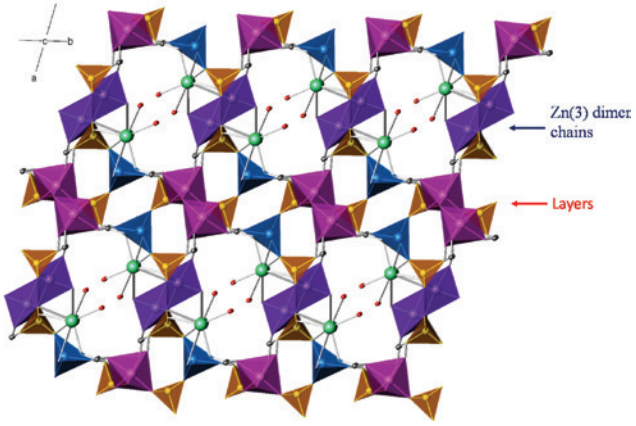

Fig. 6: View of the crystal structure of KZn_6-HPAA-3D along the c-axis: ($Zn(1)O_6$, pink octahedra; $Zn(2)O_5$ and $Zn(3)O_5$, blue and purple polyhedra; CPO_3, orange tetrahedra; O red spheres; K, green spheres and C, gray spheres).

another one from $HP(1)AA^{3-}$, and four additional oxygens from three water molecules plus a hydroxide group. Although the hydroxide anion could not be crystallographically distinguished from water molecules, it may tentatively be assigned to one of the two oxygens bridging K^+ and Zn(3) or Zn(2) metal ions (Ow1 or Ow3).

By comparison, the most significant structural differences between the anhydrous 3D $KZn(O_3PCHOHCOO)$ and the KZn_6-HPAA-3D are (a) the exclusive tetrahedral coordination around the Zn^{2+} cations, and (b) the observation that the hydroxyl group from the HPAA ligand is not coordinated to the metal ion in the former. It is worth-mentioning that there are no H-bonding networks in this anhydrous phase. When K^+ is replaced by NH_4^+ in the isostructural ammonium derivative, NH_4Zn-HPAA-3D, [20] new H-bonding interactions are formed inside the cavities between the NH_4^+ ions and the negatively charged framework. Compounds KZn_6-HPAA-3D and NH_4Zn-HPAA-3D are thermally stable, at least up to ~200 °C. Above this temperature, the solid KZn_6-HPAA-3D starts to lose water (Figure S7), an indication that the metal-coordinated water is tightly bonded to the metal centers.

Proton conductivity studies

The members of this class of coordination networks exhibit high structural versatility, acidic sites and, usually, both non-coordinating and metal-bound water molecules. All these structural features may be the basis for creating a variety of extended H-bonding networks to tune proton conductivity. Although water-mediated is the common mechanism of proton conductivity [5, 6, 9, 34], it may be enhanced by incorporating other species, such as NH_4^+/NH_3. Furthermore, post-synthesis modifications, such as ion exchange, where possible, and/or protonation through gas-solid reactions could be also, in principle, processes that could be envisaged for improving proton conduction properties [21, 35–37]. In the present study, impedance spectroscopy measurements were carried out in the range between room temperature and 80 °C at 95 % RH in order to correlate proton conductivities with structural and/or morphological changes for all synthesized solids as well as for some derivatives obtained by post-synthesis treatments by exposure to NH_3 or/and HCl gases.

Impedance spectra at different temperatures and 95 % RH are shown in Figure S8 for Mg-H_1HPAA derivatives as representative example. The total pellet resistence was calculate from the intercept of the spike or, alternatively, from the arc (low frequency end) on the Z' axis. The overall pellet conductivities for M^{2+}-H_1HPAA (M = Mg^{2+} and Zn^{2+}) compounds, in Arrhenius format, are displayed in Fig. 7.

As commented above, crystalline 1D phases can be synthesized for Mg^{2+}, Zn^{2+} from simple crystallization at room temperature. The 1D phase is not stable in the entire temperature range studied and transforms to a 2D phase that is stable, at least, up to 80 °C and 95 % RH. The 2D solids (Zn^{2+} and Mg^{2+} derivatives), either as synthesized or derived from the 1D phase, show moderate proton conductivities range between 2.1×10^{-5} S/cm

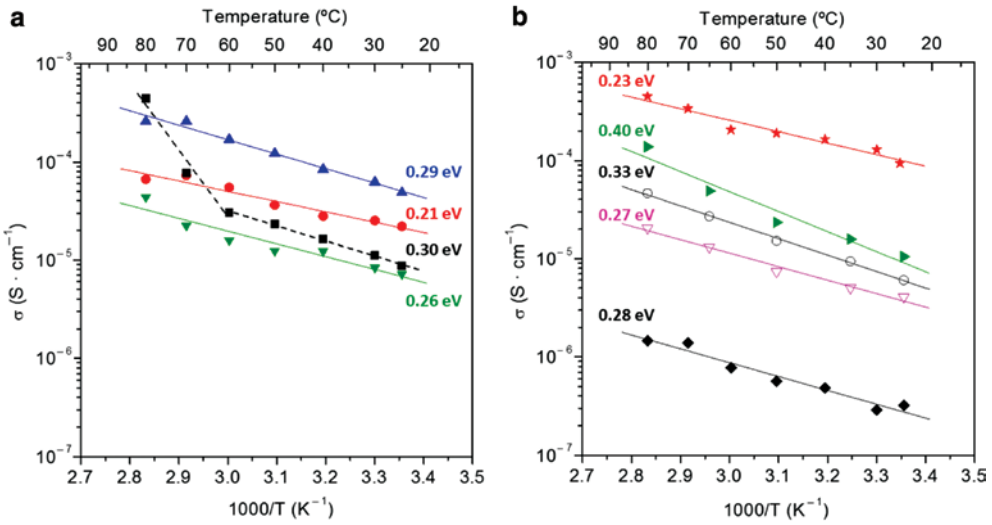

Fig. 7: Arrhenius plots for: (a) Mg-H_1HPAA derivatives [▼ Mg-H_1HPAA-2D as synthesized; ■ Mg-H_1HPAA-1D as-synthesized; ● Mg-H_1HPAA-2D after conversion; ▲ Mg-H_1HPAA-2D_NH_3] and (b) Zn-H_1HPAA derivatives [◆ KZn_6-HPAA-3D; ∇ Zn-H_1HPAA-2D as-synthesized; ○ Zn-H_1HPAA-2D_NH_3; ▶NH_4Zn-HPAA-3D; ★ Zn-H_1HPAA-2D after exposure of KZn_6-HPAA-3D to HCl(g)]. Activation energies are given for each compound.

and 6.7×10^{-5} S/cm at 80 °C and 95 % RH. The transition 1D → 2D, shown only for Mg-H_1HPAA-1D, is detected in the Arrhenius plot (Fig. 7a) as an abrupt change in the slope and, hence, in conductivity values between 80 and 60 °C (■ points). Once the 1D → 2D phase transformation has taken place, no further change in slope occurs down 60 °C. The converted 2D material exhibits a behavior practically similar to that corresponding to the as-synthetized Mg-H_1HPAA-2D solid (▼). A second cycle of measurements for the converted Mg-H_1HPAA-2D phase (●), previously checked by XRD (Figure S9), confirms a monotonic behavior in proton conductivity, similar to the as-synthesized 2D solid, over the complete range of temperature studied, the small increase observed being attributed to slight changes in morphology. This result also indicates that even if morphological changes occur, the proton conductivity is essentially an intrinsic feature of the structure of these solids. Zn-H_1HPAA-1D follows a quite similar behavior (not shown).

All the aforementioned compounds adsorb NH_3 vapors together with water from an aqueous solution. This, generally causes an increase in proton conductivity, however, an explanation of this effect is not simple. Mg-H_1HPAA-1D adsorbs a small amount of ammonia to give a compound with the stoichiometry $Mg(HO_3PCH(OH)CO_2(H_2O)_{2.6}(NH_3)_{0.2}$, Mg-$H_1$HPAA-1D_$NH_3$. The XRD pattern of this solid, Figure S10, shows splitting of diffraction peaks observed at lower angles, which may be attributed to a higher separation of the chains upon NH_3 adsorption in a relatively ordered fashion. This solid transforms to Mg-H_1HPAA-2D at high relative humidity, but still retains a small fraction of NH_3. This process causes a further enhancement of the proton conductivity (Fig. 7a, ▲ points), up to 2.6×10^{-4} S/cm, accompanied by partial amorphization of the solid, as observed by XRD (Figure S10). Since no structural changes in the crystalline 2D phase could be noted, NH_3-induced amorphization may be related to a particle size reduction. However, Zn-H_1HPAA-2D differs from Mg-H_1HPAA-2D in the capacity to adsorb NH_3. Thus, upon 3.5 h of exposure, the resulting solid, Zn-H_1HPAA-2D_NH_3, has the composition $Zn(HO_3PCHOHCO_2)(H_2O)_2(NH_3)$. As a result, proton conductivity increases slightly with respect to the as-synthesized 2D material (Fig. 7b, ○ points). No intercalation of NH_3 into the crystalline Zn-H_1HPAA-2D phase was detected by XRD but a partial solid amorphization, possibly due to particle size reduction as it was also observed for Mg-H_1HPAA-2D_NH_3. The activation energy values (Fig. 7) for these compounds fall into a range characteristic of a Grotthuss-type proton transfer mechanism, i.e. below 0.5 eV.

The 3D solids were also investigated for their proton conductivity, in order to evaluate the influence of the network architecture. These 3D frameworks present cavities containing H_2O and/or NH_4^+ guest molecules that may, in principle, contribute to establish hydrogen transport pathways and, hence to proton conductivity in different ways. The Arrhenius plots for the as-synthesized and derivatized solids are displayed in Fig. 7b.

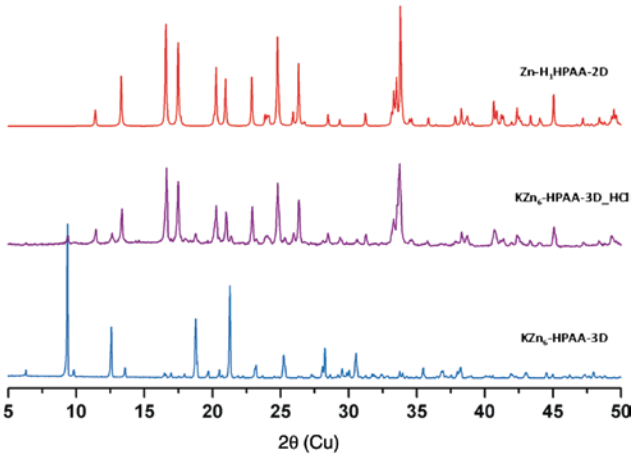

Fig. 8: X-ray powder diffraction patterns for KZn_6-HPAA-3D before and after exposure to HCl(g) (KZn_6-HPAA-3D_HCl).

Solid KZn_6-HPAA-3D (◆) exhibits a very low proton conductivity, 1.6×10^{-6} S·cm^{-1} at 80 °C and 95 % RH, due to the presence of basic groups rather than acidic groups and mobile lattice water, as happens with lower dimensionality solids. Hydrated K^+ ions are not thought to contribute to this residual conductivity as these ions occupy fixed positions in the framework playing a structural role. Given the low proton conductivity of KZn_6-HPAA-3D, the solid was put in contact with NH_3 vapors in order to increase its proton conductivity. However, no changes were found for this solid, due to the low amount of adsorbed ammonia in this relatively basic framework. Exposure of this solid to dry HCl gas led again to the phase Zn-H_1HPAA-2D as main phase, which is considered the most thermodynamically stable phase under high humidity conditions (Fig. 8). This process implies partial removal of Zn^{2+} and total depletion of K^+ ions due to ligand protonation, while the remaining Zn^{2+} ions adopt exclusively an octahedral coordination. The proton conductivity is further improved in the resulting 2D solid HCl-treated compound (★), 4.5×10^{-4} S·cm^{-1} at 80 °C and 95 % RH, as compared to the as-synthesized layered material, Zn-H_1HPAA-2D, which may be attributed to extrinsic effects caused by morphological changes upon acid treatment [38, 39].

Since NH_4Zn-HPAA-3D exhibits weak H-bonding interactions (Figure S11) an increase of the proton conductivity should be expected. As can be seen in Fig. 7b, this compound shows proton conductivity values 1.4×10^{-4} S·cm^{-1} at 80 °C and 95 % RH, two orders of magnitude higher than those of the potassium derivative. These may be rationalized with the presence of more effective proton transfer pathways in this framework, in comparison to those present in KZn_6-HPAA-3D. In these solids, a Grotthuss-type proton transfer mechanism is also observed.

Conclusions

1D and 2D $M^{2+}(OOCCH(OH)PO_3H)\cdot2H_2O$ (M^{2+} = Mg, Zn) isostructural compounds and 3D Zn^{2+}-2-hydroxyphosphonoacetate solids [$KZn_6(OOCCH(OH)PO_3)_4(OH)\cdot5H_2O$ and $NH_4Zn(OOCCH(OH)PO_3)_4$] have been prepared between room temperature and 180 °C. The aim of this study has been to correlate the structural changes with variations in proton conductivity in the range of 25–80 °C and at high RH (95 %). Under these conditions, a 1D → 2D transformation occurs about 70–80 °C. Although the stable 2D solids show moderate proton conductivities ($\sigma = 6.5\times10^{-5}$ S·cm^{-1} at 80 °C and 95 % RH), they are amenable to post synthesis modifications through gas adsorption of ammonia or HCl that appreciably enhance proton conductivity. The thermal stability of the 2D phase is further confirmed by the conversion of the 3D $KZn_6(OOCCH(OH)PO_3)_4(OH)\cdot5H_2O$, whose crystal structure has been reported by the first time in this work, to the 2D $Zn(OOCCH(OH)PO_3H)\cdot2H_2O$ upon exposure to HCl(g). All solids exhibit a Grotthuss-type proton transfer mechanism.

Acknowledgments: The work at UoC was funded by the Special Research Account (ELKE), project KA 3806. The work at UMA was funded by Spanish MINECO through MAT2013-41836-R which is co-funded by FEDER and by Junta de Andalucía through P12-FQM-1656 research projects. MBG thanks UMA Research Plan for financial support. We thank ESRF for providing synchrotron X-ray beam time on ID31.

References

[1] H. W. Langmi, J. Ren, N. M. Musyoka. in *Nanomaterials for Fuel Cell Catalysis*, K. I. Ozoemena, S. Chen (Eds.) p. 367 (Ch. 9), Springer International Publishing, Switzerland (2016).
[2] M. Yoon, K. Suh, S. Natarajan, K. Kim. *Angew. Chem. Int. Ed*. **52**, 2688 (2013).
[3] G. K. H. Shimizu, J. D. Taylor, K. W. Dawson. in *Metal Phosphonate Chemistry: From Synthesis to Applications*, A. Clearfield, K. D. Demadis (Eds.) p. 493 (Ch. 15), Royal Society of Chemistry, London (2012).
[4] P. Ramaswamy, N. E. Wong, G. K. H. Shimizu. *Chem. Soc. Rev.* **43**, 5913 (2014).
[5] J. D. Taylor, K. W. Dawson, G. K. H. Shimizu. *J. Am. Chem. Soc.* **135**, 1193 (2013).
[6] P. Ramaswamy, N. E. Wong, B. S. Gelfand, G. K. H. Shimizu. *J. Am. Chem. Soc.* **137**, 7640 (2015).
[7] S.-S. Bao, N.-Z. Li, J. M. Taylor, Y. Shen, H. Kitagawa, L.-M. Zheng, *Chem. Mater*. **27**, 8116 (2015).
[8] A. Donnadio, M. Nocchetti, F. Costantino, M. Taddei, M. Casciola, F. da Silva Lisboa, R. Vivani. *Inorg. Chem.* **53**, 13220 (2014).
[9] S. Begum, Z. Wang, A. Donnadio, F. Costantino, M. Casciola, R. Valiullin, C. Chmelik, M. Bertmer, J. Kärger, J. Haase, H. Krautscheid. *Chem. Eur. J.* **20**, 8862 (2014).
[10] K. D. Demadis, M. Papadaki, R. G. Raptis, H. J. Zhao. *Solid State Chem.* **181**, 679 (2008).
[11] K. D. Demadis, M. Papadaki, R. G. Raptis, H. Zhao. *Chem. Mater.* **20**, 4835 (2008).
[12] S. Lodhia, A. Turner, M. Papadaki, K. D. Demadis, G. B. Hix. *Cryst. Growth Des.* **9**, 1811 (2009).
[13] K. D. Demadis, M. Papadaki, M. A. G. Aranda, A. Cabeza, P. Olivera-Pastor, Y. Sanakis. *Cryst. Growth Des.* **10**, 357 (2010).
[14] R. M. P. Colodrero, P. Olivera-Pastor, A. Cabeza, M. Papadaki, K. D. Demadis, M. A. G. Aranda. *Inorg. Chem.* **49**, 761 (2010).
[15] K. D. Demadis, M. Papadaki, I. Cisarova. *ACS-Appl. Mater. Interf.* **2**, 1814 (2010).
[16] R. M. P. Colodrero, A. Cabeza, P. Olivera-Pastor, J. Rius, D. Choquesillo-Lazarte, J. M. García-Ruiz, M. Papadaki, K. D. Demadis, M. A. G. Aranda. *Cryst. Growth Des.* **11**, 1713 (2011).
[17] R. M. P. Colodrero, A. Cabeza, P. Olivera-Pastor, E. R. Losilla, K. E. Papathanasiou, N. Stavgianoudaki, J. Sanz, I. Sobrados, D. Choquesillo-Lazarte, J. M. García-Ruiz, L. León Reina, M. A. G. Aranda, P. A. Corvillo, K. D. Demadis. *Chem. Mater.* **24**, 3780 (2012).
[18] M. Bazaga-García, M. Papadaki, R. M. P. Colodrero, P. Olivera-Pastor, E. R. Losilla, B. Nieto-Ortega, M. A. G. Aranda, D. Choquesillo-Lazarte, A. Cabeza, K. D. Demadis. *Chem. Mater.* **27**, 424 (2015).
[19] R. Fu, S- Xiang, H. Zhang, J. Zhang, X. Wu. *Crystal Growth & Design* **5**, 1795 (2005).
[20] R. Fu, H. Zhang, L. Wang, S. Hu, Y. Li, X. Huang, X. Wu. *Eur. J. Inorg. Chem.* **16**, 3211 (2005).
[21] M. Bazaga-García, R. M. P. Colodrero, M. Papadaki, P. Garczarek, J. Zoń, P. Olivera-Pástor, E. R. Losilla, L. León-Reina, M. A. G. Aranda, D. Choquesillo-Lazarte, K. D. Demadis, A. Cabeza. *J. Am. Chem. Soc.* **136**, 5731 (2014).
[22] A. Boultif, D. Louer. *J. Appl. Cryst.* **37**, 724 (2004).
[23] J. Rius, O. Vallcorba, I. Peral, C. Frontera, C. Miravitlles. DAjust Software. "*Pattern matching, space group determination and intesity extraction from powder diffraction data*", Instituto de Ciencias de los Materiales de Barcelona (CSIC), Spain (2011).
[24] J. Rius. *Acta Cryst.* **A67**, 63 (2011).
[25] H. M. Rietveld. *J. Appl. Cryst.* **2**, 65 (1969).
[26] A. C. Larson, R. B. Von Dreele. "*General Structure Analysis System (GSAS)*", Los Alamos National Laboratory Report LAUR 86–748 (2004).
[27] B. H. Toby. *J. Appl. Cryst.* **34**, 210 (2001).
[28] winDETA; Novocontrol GmbH: Hundsangen, Germany (1995).
[29] A. Cabeza, M. A. G. Aranda. in *Metal Phosphonate Chemistry: From synthesis to Applications*, A. Clearfield, K. D. Demadis (Eds.) p. 107 (Ch. 4), *The Royal Society of Chemistry*, London (2012).
[30] A. Cabeza, P. Olivera-Pastor, R. M. P. Colodrero. in *Tailored Organic-Inorganic Materials*, E. Brunet, J. L. Colón, A. Clearfield (Eds.) p. 137 (Ch. 4), John Wiley & Sons, Inc., Hoboken, New Jersey (2015).
[31] K. D. Demadis, A. Panera, Z. Anagnostou, D. Varouhas, A. M. Kirillov, I. Cisarova. *Cryst. Growth Des.* **13**, 4480, (2013).
[32] R. Fu, S. Hu, X. Wu. *Dalton Trans.* **43**, 9440 (2009).
[33] Z. Sun, H. Chen, Z. Liu, L. Cui, Y. Zhu, Y. Zhao, J. Zhang, W. You, Z. Zhu. *Inorg. Chem. Commun.* **10**, 283–286 (2007).
[34] D. D. Borges, S. Devautour-Vinot, H. Jobic, J. Olivier, F. Nouar, R. Semino, T. Devic, C. Serre, F. Paesani, G. Maurin. *Angew. Chem. Int. Ed.* **55**, 3919 (2016).

[35] E. Pardo, C. Train, G. Gontard, K. Boubekeur, O. Fabelo, H. Liu, B. Dkhil, F. Lloret, K. Nakagawa, H. Tokoro, S.-I. Ohkoshi, M. Verdaguer. *J. Am. Chem. Soc* **133**, 15328 (2011).
[36] S. Liu, Z. Yue, Y. Liu. *Dalton Trans.* **44**, 12976 (2015).
[37] S.-N. Zhao, X.-Z. Song, M. Zhu, X. Meng, L.-L. Wu, S.-Y. Song, C. Wang, H.-J. Zhang. *Dalton Trans.* **44**, 948 (2015).
[38] M. Taddei, A. Donnadio, F. Costantino, R. Vivani, M. Casciola. *Inorg. Chem.* **52**, 12131 (2013).
[39] S. Tominaka, A. K. Cheetham, *RSC Adv.* **4**, 54382 (2014).

Supplemental Material: The online version of this article (DOI: 10.1515/pac-2016-1003) offers supplementary material, available to authorized users.